Ferromagnetism and canted spin phase in AlAs/$Ga_{1-x}Mn_xAs$ single quantum wells: Monte Carlo simulation

M. A. Boselli
Instituto de Física, Universidade do Estado do Rio de Janeiro, Rua São Francisco Xavier 524, 20.500-013 Rio de Janeiro, R.J., Brazil

A. Ghazali
Groupe de Physique des Solides, Universités Paris 7 et Paris 6 Tour 23, 2 Place Jussieu, F-75 125 Paris Cedex 05, France

I. C. da Cunha Lima
Instituto de Física, Universidade do Estado do Rio de Janeiro, Rua São Francisco Xavier 524, 20.500-013 Rio de Janeiro, R.J., Brazil

(Received 16 February 2000)

The magnetic order resulting from a confinement-adapted Ruderman-Kittel-Kasuya-Yosida indirect exchange between magnetic moments in the metallic phase of a AlAs/$Ga_{1-x}Mn_xAs$ quantum well is studied by Monte Carlo simulation. This coupling mechanism involves magnetic moments and carriers (holes), both coming from the same Mn^{2+} ions. It leads to a paramagnetic, a ferromagnetic, or a canted spin phase, depending on the carrier concentration, and on the magnetic layer width. It is shown that high transition temperatures may be obtained.

I. INTRODUCTION

During the last decade, due to the advances in the control of materials growth, and also in the techniques of characterization, a new interest arose in the study of the magnetic order in layered materials. This area is not restricted to magnetism in metals, but it also includes the study of magnetic semiconductor pseudobinary alloys like $A_{1-x}M_xB$, where M stands for a magnetic ion. These alloys are called diluted magnetic semiconductors (DMSs).[1,2]

Recently some groups[3–9] succeeded in producing homogeneous samples of $Ga_{1-x}Mn_xAs$ alloys with x up to 7% using low-temperature (200–300 °C) (MBE) molecular beam epitaxy techniques. Mn is a transition metal having its $3d$ level partially filled with five electrons, in such a way that it carries a magnetic moment of $5\hbar/2$, according to Hund's rule. In the insulating phase, as in II-VI DMSs, two Mn^{2+} ions occupying the nearest-neighbor positions are assumed to interact with each other via a superexchange mechanism, resulting in an antiferromagnetic ordering of their magnetic moments. In the fcc alloys, these interactions are frustrated, establishing the possibility of settling a spin-glass phase at low temperature. A double-exchange mechanism which might stabilize the ferromagnetic coupling between the Mn ions in III-V DMSs has been suggested by Akai,[10] but has not been confirmed in the electron paramagnetic resonance (EPR) experiments performed by Szczytko *et al.*,[11] who did not observe the trace of neutral Mn, concluding that the double-exchange mechanism is not effective.

The possibility of having a DMS based on GaAs opens a wide range of potential applications such as integrated magneto-optoelectronic devices. Besides its practical importance, this kind of DMS introduces an interesting problem: an Mn impurity in GaAs is an acceptor (it binds one hole), and at the same time it carries a localized magnetic moment. In the $Ga_{1-x}Mn_xAs$ alloy Mn is, in fact, a strong p dopant,[3,7] the free hole concentration reaching even 10^{20-21} cm^{-3}. At small Mn concentrations, the alloy is a paramagnetic insulator. As x increases it becomes ferromagnetic, going through a nonmetal-to-metal transition for higher concentrations and keeping its ferromagnetic phase. For x above 5%, the alloy becomes a ferromagnetic insulator.[7] In the metallic phase, depending on the value of x, the temperature of the ferromagnetic transition is observed in the range of 30–100 K, the highest values observed in DMSs. The ferromagnetic order in the metallic phase is understood, at present, as resulting from the indirect exchange between the Mn^{2+} ions due to the spin polarization of the hole gas.

The aim of this work is to study the magnetic order resulting from the indirect exchange between magnetic moments in a AlAs/$Ga_{1-x}Mn_xAs$ quantum well. A confinement-adapted Ruderman-Kittel-Kasuya-Yosida[12–15] (RKKY) mechanism is believed to be the most important interaction in such systems, if sufficiently strong doping is provided, as is the case in metallic samples. It leads to an indirect exchange coupling between Mn^{2+} ions, mediated by carriers (holes), which come from the same Mn^{2+} ions.

This article is organized as follows. In Sec. II we present the calculation of the RKKY exchange for a confined Fermi gas in a semiconductor heterostructure. For the sake of relating our results with other previous ones, we explicitly separate our calculations as intrasubband and intersubband contributions. We emphasize that, in the quantum limit, i.e., when only the first subband is occupied, the intrasubband exchange is factorized into a purely two-dimensional (2D) RKKY exchange times a form factor determined by the architecture of the confining structure.[16]

In Sec. III a Monte Carlo simulation is performed to determine the resulting magnetic phases and the relevant properties. Our calculations reveal that a ferromagnetic order may

occur in a single DMS quantum well only beyond a minimum width of the magnetic layer; otherwise the sample is paramagnetic. This is in keeping with recent experiments,[17] and is a consequence of the need for a certain number of magnetic neighbors before a ferromagnetic phase settles in. Depending on the well width and on the effective two-dimensional carrier concentration, a canted phase can occur, with a sizable net low-temperature magnetization $\langle S\rangle/S_{max}$ and a well-behaved Edwards-Anderson order parameter q. The magnetic susceptibilities are calculated in the existing phases. Finally, in Sec. IV we summarize the results obtained, and comment on the expected magnetic order in the structures analyzed.

II. RKKY INTERACTION IN A QUANTUM WELL

The RKKY interaction between localized magnetic moments embedded in a Fermi gas is a well-understood problem, since its early developments almost 50 years ago. However, new areas for experimental research brought into evidence some theoretical problems concerning the RKKY interaction in low-dimensional systems, so far unexplored, such as purely 2D and 1D arrangements of magnetic moments, interaction between magnetic layers, magnetic moments in inhomogeneous electron gas, etc.[18–26] The indirect exchange between localized magnetic moments in a quantum well mediated by a Fermi gas has been addressed several times. Basically, it deals with a confined electron (or hole) gas, therefore a quasi-two-dimensional system, being locally polarized by magnetic moments distributed in a layer. To our knowledge, Korenblit and Shender[27] were the first to obtain a closed expression to the equivalent of the RKKY interaction in the limiting situation of a purely 2D electron gas, although Kittel[15] obtained a numerical solution to this question earlier. Larsen[28] derived an expression for a general dimensionality, reproducing the Korenblit-Shender results for $d=2$. A detailed calculation to obtain a closed expression in 2D was shown by Béal-Monod.[29] Gummich and da Cunha Lima[30] studied the indirect exchange between magnetic impurities in a doped GaAs/AlAs quantum well in the diluted regime, obtaining a ferromagnetic interaction. Finally, another expression for a generic dimensionality has been derived by Aristov.[31] The approximation of the Fermi gas in a quantum well by a purely 2D system is seldom a reasonable choice. Helman and Baltensperger[24,25] treated the question of the polarization of an inhomogeneous electron gas in several circumstances, emphasizing the roles of the confined and extended states. The specific case of a DMS quantum well was addressed recently by Dietl *et al.*,[32] but they assumed that the magnetic moments are spread all over the region allowed to the carriers, and in that case the intersubband contributions to the Curie-Weiss temperature cancel out in a mean-field approximation.

The interaction potential between a Fermi gas and a set of localized magnetic moments at positions $\vec{R}_i$ is well described by the Hund-type exchange potential

$$H_{\rm ex}=-I\sum_i \vec{S}_i\cdot\vec{s}(\vec{r})\,\delta(\vec{r}-\vec{R}_i), \tag{1}$$

where $\vec{S}_i$ is the spin of the magnetic moment at position $\vec{R}_i$, which will be treated as a classical variable, and $\vec{s}(\vec{r})$ is the spin operator of the fermion at $\vec{r}$. Here I is the sp-d interaction.[33] If $\hat{\psi}_\sigma(\vec{r})$ and $\hat{\psi}^\dagger_\sigma(\vec{r})$ describe the fermion field operator for spin σ, then

$$s^z(\vec{r})=\frac{1}{2}[\,\hat{\psi}^\dagger_\uparrow(\vec{r})\,\hat{\psi}_\uparrow(\vec{r})-\hat{\psi}^\dagger_\downarrow(\vec{r})\,\hat{\psi}_\downarrow(\vec{r})\,], \tag{2}$$

$$s^+(\vec{r})=\hat{\psi}^\dagger_\uparrow(\vec{r})\,\hat{\psi}_\downarrow(\vec{r}), \tag{3}$$

$$s^-(\vec{r})=\hat{\psi}^\dagger_\downarrow(\vec{r})\,\hat{\psi}_\uparrow(\vec{r}), \tag{4}$$

with the usual definitions of $s^+=s_x+is_y$, and $s^-=s_x-is_y$. Instead of free fermions in a 3D space, the electrons and holes in a semiconductor heterostructure are confined in the growth direction, assumed to be the z axis, due to the mismatch of the conduction and valence band edges. Since they are free particles in the plane perpendicular to that growth direction, i.e., in the plane parallel to the semiconductor interfaces, their field operators are given by

$$\hat{\psi}_\sigma(\vec{r})=\frac{1}{\sqrt{A}}\sum_{n,\vec{k}} e^{i\vec{k}.\vec{R}}\phi_n(z)\,\eta c_{n,\vec{k},\sigma}, \tag{5}$$

where A is the normalization area, $\vec{k}$ is a wave vector in the plane (x,y), η is the spin tensor, $\phi_n(z)$ is the envelope function which describes the motion of the fermion in the z direction, and $c_{n,\vec{k},\sigma}$ is the fermion annihilation operator for the state $(n,\vec{k},\sigma)$. Here $\vec{R}$ represents a vector in the 2D coordinates plane (x,y). The usual RKKY perturbation calculation up to second order leads to the correction on the ground-state energy of the system formed by the set of (classical) localized moments and the Fermi gas:

$$\delta E^{(2)}=\delta E^{(2)}_a+\delta E^{(2)}_b, \tag{6}$$

where

$$\delta E^{(2)}_a=-\left(\frac{I}{2N}\right)^2\sum_i\sum_{n,n'}|\phi_n(z_i)|^2|\phi_{n'}(z_i)|^2 \times S_i(S_i+1)\sum_{\vec{q}}\chi^{n,n'}(\vec{q}), \tag{7}$$

and

$$\delta E^{(2)}_b=-\left(\frac{I}{2N}\right)^2\sum_j\sum_{i\neq j}\sum_{n,n'}\sum_{\vec{q}}2\ \mathrm{Re}[\,\phi^*_n(z_i)\phi_{n'}(z_i) \times\phi^*_{n'}(z_j)\phi_n(z_j)e^{-i\vec{q}.(\vec{R}_i-\vec{R}_j)}]\chi^{n,n'}(\vec{q})\vec{S}_i\cdot\vec{S}_j. \tag{8}$$

Equations (7) and (8) are, respectively, the self-energy term and the RKKY exchange in the form they assume for confined fermions. The coordinates $(\vec{R}_i,z_i)$ describe the position of the impurity i in the plane (x,y) and in the growth direction; $\vec{q}$ is a two-dimensional wave vector. $\chi^{n,n'}(\vec{q})$ is the equivalent to the Lindhard function:[34,35]

$$\chi^{n,n'}(\vec{q})=\sum_{\vec{k}}\frac{\theta(E_F-\epsilon_{n,\vec{k}})-\theta(E_F-\epsilon_{n',\vec{k}+\vec{q}})}{\epsilon_{n',\vec{k}+\vec{q}}-\epsilon_{n,\vec{k}}}. \quad (9)$$

Equations (7) and (8) are used to define the exchange Hamiltonian

$$H_{\rm ex}=-\sum_{i,j} J_{ij}\vec{S}_i\cdot\vec{S}_j. \quad (10)$$

For $i\neq j$,

$$J_{ij}=\left(\frac{I}{2A}\right)^2\sum_{n,n'}\sum_{\vec{q}} 2\mathrm{Re}[\phi_n^*(z_i)\phi_{n'}(z_i)\phi_{n'}^*(z_j)\times\phi_n(z_j)e^{-i\vec{q}\cdot(\vec{R}_i-\vec{R}_j)}]\chi^{n,n'}(\vec{q}). \quad (11)$$

A. Intrasubband terms

To our knowledge, complete calculations of Eq. (8) have only been performed for intrasubband transitions, using different approaches. For the sake of completeness, we will show how this is achieved in our treatment. The contribution of a subband n to the exchange reads:

$$J_{ij}^{(n)}=\left(\frac{I}{2A}\right)^2|\phi_n(z_i)|^2|\phi_n(z_j)|^2\sum_{\vec{q}} 2\cos(\vec{q}\cdot\vec{R}_{ij})\chi^{n,n}(\vec{q}). \quad (12)$$

We observe that, in the so-called quantum limit, when only the first subband ($n=0$) is occupied, the difference between Eq. (12) and the indirect exchange mediated by a 2D electron gas comes from the nonuniform charge density in the confining direction z. Actually, in that case, Eq. (12) factorizes into a form factor $\mathcal{F}^{ij}$ and a purely 2D exchange:[16]

$$J_{ij}^{(0)}=\mathcal{F}^{ij}J_{ij}^{(2-D)}, \quad (13)$$

where

$$\mathcal{F}^{ij}=|\phi_0(z_i)|^2|\phi_0(z_j)|^2 \quad (14)$$

and

$$J_{ij}^{2-D}=\left(\frac{I}{2A}\right)^2\sum_{\vec{q}} 2\cos(\vec{q}\cdot\vec{R}_{ij})\chi^{n,n}(\vec{q}). \quad (15)$$

It is easy to show, by using the dimensionless variables $x=kR_{ij}$ and $y=qR_{ij}$, that the Fourier transform of the modified Lindhard function, appearing in the summation in $\vec{q}$ on the right-hand side (RHS) of Eq. (12), becomes

$$\chi^n(R_{ij})=\frac{4m_t^*A^2}{\pi^3\hbar^2R_{ij}^2}\int_0^\infty dyyJ_0(y)\int_0^{k_F^{(n)}R_{ij}}dxx\times\int_0^{\pi/2}d\phi\frac{1}{y^2-4x^2\cos^2\phi}, \quad (16)$$

where $\chi^n(R_{ij})=\Sigma_{\vec{q}}2\cos(\vec{q}\cdot\vec{R}_{ij})\chi^{n,n}(\vec{q})$. The transversal effective mass m_t^* is assumed as isotropic in the plane parallel to the interfaces. As usual, $k_F^{(n)}=\sqrt{2m_t^*(E_F-\epsilon_n)}/\hbar$. Performing the ϕ integration and changing variables again ($y/2x\rightarrow y$),

$$\chi^n(R_{ij})=\frac{2m_t^*A^2}{\pi^2\hbar^2R_{ij}^2}\int_0^{k_F^{(n)}R_{ij}}dxx\int_1^\infty dyJ_0(2xy)\frac{1}{\sqrt{y^2-1}}. \quad (17)$$

The integral on y is straightforward:[36]

$$\chi^n(R_{ij})=-\frac{m_t^*A^2}{\pi\hbar^2R_{ij}^2}\int_0^{k_F^{(n)}R_{ij}}dxxJ_0(x)N_0(x). \quad (18)$$

After performing the integral on x, Eq. (18) results in

$$\chi^n(R_{ij})=-\frac{m_t^*A^2}{\pi\hbar^2}k_F^{(n)2}[J_0(k_F^{(n)}R_{ij})N_0(k_F^{(n)}R_{ij})+J_1(k_F^{(n)}R_{ij})N_1(k_F^{(n)}R_{ij})]. \quad (19)$$

This expression for the real-space Lindhard function has been derived in a different context, by several authors.[27,30,29,31,37] The final expression for the intrasubband exchange becomes

$$J_{ij}^{(n)}=-\left(\frac{I}{2}\right)^2\frac{m_t^*}{\pi\hbar^2}k_F^{(n)2}|\phi_n(z_i)|^2|\phi_n(z_j)|^2\times[J_0(k_F^{(n)}R_{ij})N_0(k_F^{(n)}R_{ij})+J_1(k_F^{(n)}R_{ij})N_1(k_F^{(n)}R_{ij})]. \quad (20)$$

B. Intersubband terms

The contribution of the intersubband terms cannot be expressed easily in a closed form. Starting over from Eq. (11), and using the same approach as in Ref. 13, we arrive at

$$J_{ij}^{(n,n')}=\left(\frac{I}{2}\right)^2\frac{1}{\pi}\mathrm{Re}[\phi_{n'}^*(z_i)\phi_n(z_i)\phi_n^*(z_j)\phi_{n'}(z_j)]\times\int_0^\infty dqqF_{n,n'}(q)J_0(qR_{ij}), \quad (21)$$

where we used

$$F_{n,n'}(q)=\frac{m_t^*}{\hbar^2}\frac{1}{\pi^2}\int d^2k\times\frac{q^2+\Delta_{n',n}}{(q^2+\Delta_{n',n})^2-(2\vec{k}\cdot\vec{q})^2}\theta(\epsilon_{n'}-E_F), \quad (22)$$

and $\Delta_{n',n}=2m_t^*(E_{n'}-E_n)/\hbar^2$. The integral in Eq. (22) is, then, straightforward:

$$F_{n,n'}(q)=\frac{m_t^*}{2\pi\hbar^2}\left(1-\frac{\Delta_{n',n}}{q^2}\right)\times\left[1-\sqrt{1-\left(\frac{2k_F^{(n)}q}{q^2+\Delta_{n',n}}\right)^2}\times\theta(q^2+\Delta_{n',n}-2qk_F^{(n)})\right]\theta(\epsilon_{n'}-E_F). \quad (23)$$

III. MONTE CARLO SIMULATION: MAGNETIC ORDERING

In order to determine the possible magnetic order in GaAs:Mn quantum wells, we have performed extensive Monte Carlo simulations. Classical spins $\mathbf{S}_i$, randomly distributed on the cation sites with concentration x, are assumed to interact through the RKKY exchange Hamiltonian defined by Eq. (10).

In the present work we have focused our attention on metallic single quantum wells with Mn concentration $x=5\%$, and we have neglected possible (anti)ferromagnetic interactions between the nearest-neighbor and the next-nearest-neighbor pairs. The RKKY exchange interaction derived in Sec. II is assumed to be effective within a cutoff radius which we have taken as $R_c=4a$, $R_c=2a$, and $R_c=a$, where a is the fcc lattice parameter of GaAs. This makes the smallest value assumed for R_c nearly equal to the hole mean free path estimated from bulk transport measurements.[7] The highest value $R_c=2.2$ nm amounts to three to four values of that mean free path. The consequences of the cutoff radius on the results will be discussed below.

The calculation is performed in a finite box, whose axes are parallel to the [100] directions. Its dimensions are $L_x=L_y$ and $L_z=Na/2$, and N is the number of DMS monolayers (ML) in the well. Periodic boundary conditions are imposed in the (x,y) plane. The lateral dimensions are adjusted in such a way that the total number N_s of spins is about 4400, for all samples with different L_z. The initial spin orientations are randomly assigned. At a given temperature, the energy of the system due to the RKKY interaction is calculated, and the equilibrium state for a given temperature is sought by changing the individual spin orientation according to the Metropolis algorithm.[37,38] A slow cooling stepwise process is accomplished making sure that the thermal equilibrium is reached at every temperature. The resulting spin configuration is taken as the starting configuration for the next step at a lower temperature.

For every temperature, the average magnetization $\langle M\rangle$ and the Edwards-Anderson (EA) order parameter q are calculated.[38] The latter is defined as

$$q=\frac{1}{N}\sum_{i=1}^{N}\left(\sum_{\alpha}\left|\frac{1}{t}\sum_{t'=t_0}^{t_0+t}S_{i\alpha}(t')\right|^2\right)^{1/2}, \tag{24}$$

where $\alpha=x$, y, and z. In order to avoid spurious results in obtaining the average over a large time interval t, a summation on t' is performed starting from a time t_0, when the system already reached the thermal equilibrium.

In our calculations we used the value $N_0\beta=-1.2$ eV, taken from Ref. 39, for which we obtain transition temperatures in good agreement with the experimental data. Recently, the value $N_0\beta=-0.9$ eV has been obtained theoretically,[40] confirming the result of Ref. 39. The earlier estimate[7] $|N_0\beta|=3.3$ eV is probably too high.

Monte Carlo calculations have been performed in 16 samples, as shown in Table I, the well widths varying from 25 Å to 100 Å (from 9 ML to 35 ML). In sample No. 1, for a well width of 50 Å , and assuming $R_c=8$ ML, we tested the effect of a small hole concentration, making p just 1% of x. This amounts to $p\approx 1.1\times 10^{19}$ cm^{-3}. We found that the spins can be arranged in a ferromagnetic phase even at this carrier concentration. For that sample the calculation gives a transition temperature near 27 K.

TABLE I. Sample characteristics: L is the well width, r is the ratio of the carrier concentration to the Mn concentration, T_c is the transition temperature for the phases: F, ferromagnetic; P, paramagnetic; C, canted spin. R_c is the cutoff radius of the RKKY interaction, in number of monolayers.

Sample No.	L (Å)	r	R_c	Phase	T_c (K)
1	50	0.01	8	F	27
2	25	0.10	8	P	$\leqslant 1$
3	35	0.10	8	F	50
4	50	0.10	8	F	50
5	60	0.10	8	C	50
6	80	0.10	8	F	50
7	100	0.10	8	C	40
8	25	0.25	8	F	50
9	35	0.25	8	F	50
10	50	0.25	8	C	50
11	60	0.25	8	C	40
12	100	0.25	8	C	30
13	60	0.25	2	P	$\leqslant 1$
14	80	0.25	2	P	$\leqslant 1$
15	60	0.25	4	F	35
16	80	0.25	4	F	80

In Fig. 1 the normalized average magnetization is shown for sample No. 2–7 with different well widths, but with a fixed carrier concentration of 10% of x, i.e., $p\approx 1.1\times 10^{20}$ cm^{-3}, and the same cutoff $R_c=8$ ML. For a very thin well (25 Å), we found that the sample is paramagnetic. The EA order parameter for these samples is shown in Fig. 2. It can be observed that, for sample No. 2, there is no phase transition. All the other curves in Fig. 2 (samples Nos. 3–7) are characteristic of an ordered phase. Raising the well width (starting from 35 Å), the number of interacting neighbors increases, and the sample shows successively a ferromagnetic phase (sample Nos. 3, 4, and 6) and a canted spin

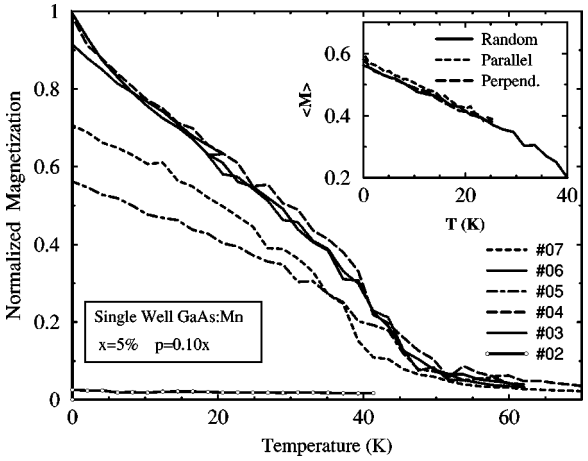

FIG. 1. Normalized magnetization vs temperature for sample Nos. 2–7 indicated in Table I. The inset shows the low-temperature magnetization with three starting spin configurations: random, parallel, and normal to the layers.

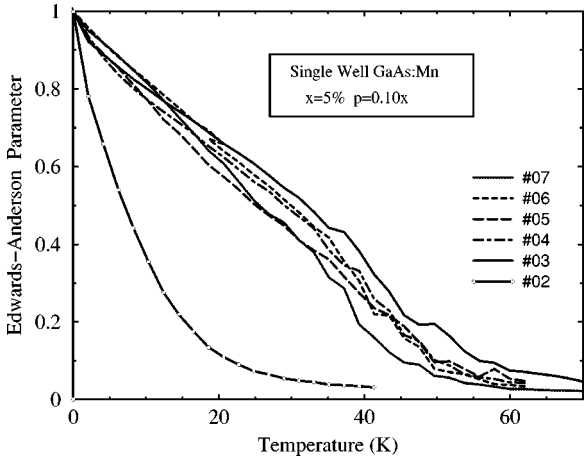

FIG. 2. EA parameter vs temperature for sample Nos. 2–7 indicated in Table I.

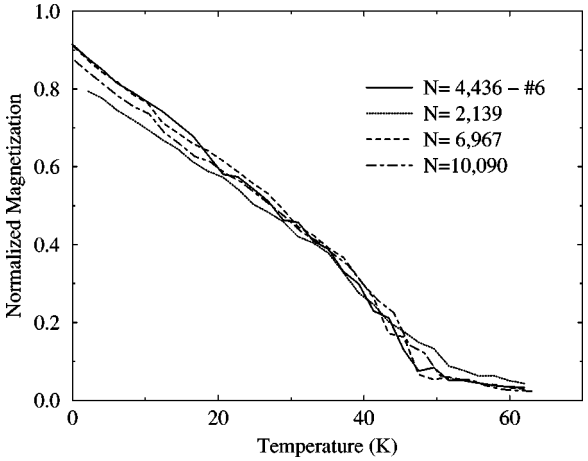

FIG. 3. Size test for the normalized magnetization vs temperature in different samples with the same characteristics as sample No. 6 but with different total number of magnetic moments. The solid line repeats the previous results for sample No. 6 ($N=4436$); dotted line, $N=2139$; dashed line, $N=6967$; dash-dotted line, $N=10\,090$.

arrangement (sample Nos. 5 and 7). The value chosen for the cutoff radius is larger than the first zero of the J_{ij}^{RKKY}, so antiferromagnetic interactions are turned on. With these choices of p and R_c, depending on the well width, the antiferromagnetic interactions can settle a fraction of the Mn magnetic moments antiparallel. This is the origin of the canted spin phase. The final average magnetizations in Fig. 1 at $T=0$ K are only a fraction of the maximum magnetization, around 60% for sample No. 5 and 70% for sample No. 7. The transition temperatures were found in the range of 40–50 K. No spin-glass phase with vanishing magnetization was found.

The existence of the canted phase requires a careful analysis of a possible dependence on the cooling process initial conditions. In order to clarify that point, we performed two additional simulations on sample No. 5, starting at $T=25$ K, where the sample shows already a significant partial alignment of spins, and we proceeded with a slow cooling-down process. In the first simulation, we assumed a starting configuration in which all spins are aligned perpendicularly to the interface. In the second, the spin alignment is made parallel to the interfaces. This choice of a rather low starting temperature for cooling is necessary; otherwise the thermal excitation would immediately randomize the initial configuration. The results are shown in the inset of Fig. 1. We observe that the appearance of the canted phase does not depend on the choice of the starting configuration, and the three simulations converge, within statistical fluctuations, to the same value of the magnetization at every temperature step.

At low temperature in ferromagnetic samples, the spin-spin correlation function $\langle \vec{S}_i \cdot \vec{S}_j \rangle \rightarrow 1$. In canted spin phases, however, the spins are not all collinear, and the spin-spin correlation function changes from layer to layer, reflecting the nonuniformity in the z direction. This effect is really due to the RKKY exchange couplings in those samples. For the sake of completeness, we considered also four different samples of sizes $N=2139$, $N=4436$ (sample No. 6), $N=6967$, and $N=10\,090$, respectively, with the same Mn content, the same carrier concentration, and the same well width. As can be seen in Fig. 3, apart from a slight deviation for the smallest sample with $N=2139$, all other samples not only have nearly the same magnetization curve as a function of temperature, within statistical fluctuations, but they present the same magnetization profile along the z axis (not shown in the figure). These results also show that finite-size effects are negligible for large enough samples ($N \geqslant 4000$). We also notice the important result that the Curie temperature and the nature of magnetic ordering are not affected by size effects. A similar size test has been performed for sample No. 5 with the same conclusions.

In Fig. 4 the magnetization as a function of temperature is shown for sample Nos. 8–12, with a higher carrier concentration $p=0.25x$, but keeping the same cutoff radius of 8 ML. The EA order parameter for these samples shown in Fig. 5 as a function of temperature, gives evidence for the existence of ordered phases. The Fermi wave number increases with carrier concentration, which decreases the in-plane distance corresponding to the first zero of the RKKY interaction. In consequence, in some samples, the magnetic moments order in the canted spin phase (sample Nos. 10–12). In other samples, however, the ferromagnetic interaction prevails and the total magnetization is reached (sample Nos.

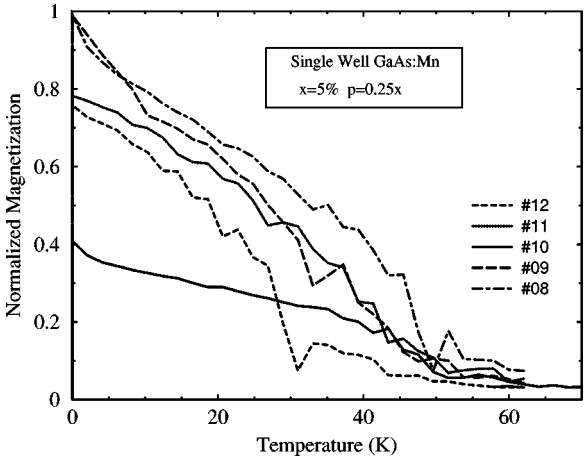

FIG. 4. Normalized magnetization vs temperature for sample Nos. 8–12 indicated in Table I.

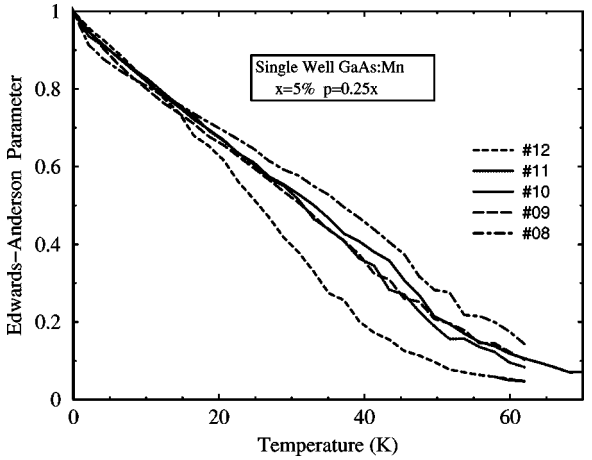

FIG. 5. EA parameter vs temperature for sample Nos. 8–12 indicated in Table I.

8 and 9). Notice that the canted phase appears here already for $L=50$ Å , while the phase is still ferromagnetic for that width when $p=0.1x$. The transition temperatures were estimated to lie between 30 K and 50 K.

In Fig. 6 we explored the effect of the cutoff radius on the spin ordering with $p=0.25x$. A cutoff radius $R_c=2$ ML was used in sample No. 13 ($L=60$ Å) and No. 14 ($L=80$ Å), while $R_c=4$ ML was used in sample No. 15 ($L=60$ Å) and No. 16 ($L=80$ Å). The former is too small, resulting in the fact that no net magnetization is allowed. The respective EA order parameters (Fig. 7) are typical of a paramagnetic phases for sample Nos. 13 and 14. The choice of a larger R_c ordered spins in a ferromagnetic phase, with transition temperatures calculated to be 35 K for sample No. 15 and 80 K for sample No. 16. The cutoff radius of 4 ML is smaller than the first zero of J_{ij}^{RKKY}. In this situation the canted spin arrangement is not allowed, and the sample can be either paramagnetic or ferromagnetic.

Finally in Fig. 8 the magnetic susceptibility for sample No. 7 is presented, calculated from the equilibrium magnetization fluctuations. Notice that the peak in the susceptibility indicates the same T_c as estimated from the magnetizations and EA order parameter curves (Figs. 1 and 2, respectively).

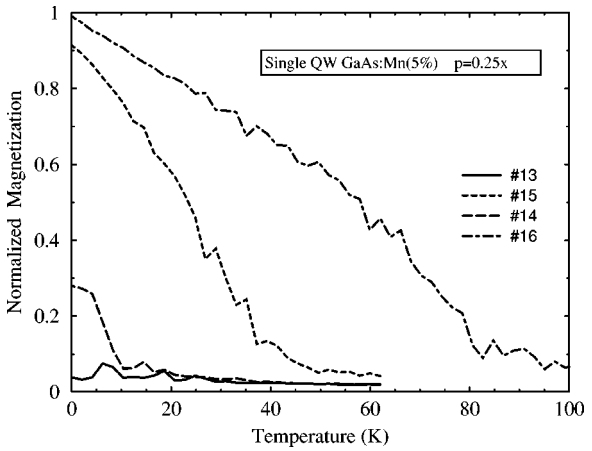

FIG. 6. Normalized magnetization vs temperature for sample Nos. 13–16 indicated in Table I.

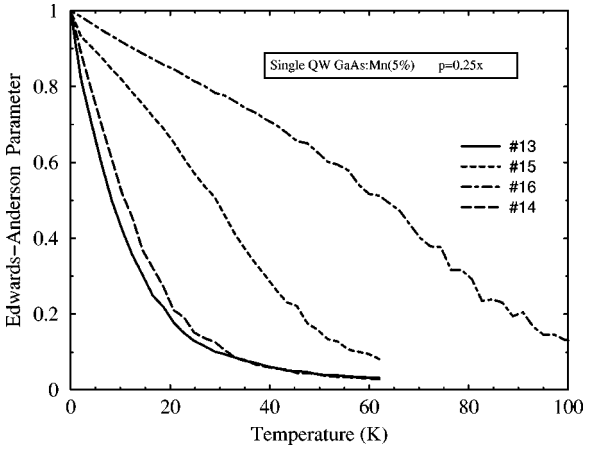

FIG. 7. EA parameter vs temperature for sample Nos. 13–16 indicated in Table I.

IV. DISCUSSIONS AND FINAL COMMENTS

The results of the Monte Carlo simulations indicate that, besides the choice of the range of the interaction (the cutoff radius R_c), two parameters are determined in the magnetic ordering in these heterostructures: the magnetic layer width L and the carrier concentration p.

It is observed from resistivity measurements that the holes have a small mean free path[7,41] in these materials. The criteria for choosing the cutoff in a Monte Carlo simulation must take into account the natural scales of the interaction. These scales are the transport mean free path (since the RKKY interaction is based on the very existence of free carriers) and also the spin coherence length. We tested different R_c's in the range of the mean free path estimated from resistivity data. The influence of this parameter on the magnetic order is simple. If R_c is smaller than the first zero of J_{ij}^{RKKY} (a proper choice for the case in which the transport mean free path or the spin coherence length are small), there are two possibilities of magnetic order: ferromagnetic or paramagnetic. For larger R_c, on the other hand, corresponding to the cases where both the transport mean free path and the coherence length are large, a canted magnetization may be observed.

In all the explored samples, no spin-glass phase was

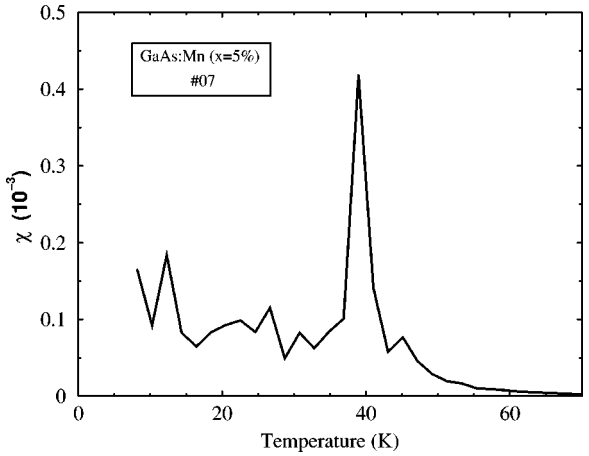

FIG. 8. Magnetic susceptibility vs temperature, calculated from equilibrium magnetization fluctuations, for sample No. 7 indicated in Table I.

found. This is presumably due to the fact that while spin frustration exists, as witnessed by the occurrence of canted spin phases, it is not strong enough to produce a spin-glass phase, as in canonical metallic spin glasses. A spin-glass phase in these DMS structures would probably require a much higher carrier concentration.

In what concerns the influence of the width of the quantum well, we conclude that, for thin layers, the number of interacting ions is small within the cutoff radius and the sample is paramagnetic. When L becomes larger, the number of interacting ions increases and a collective magnetic ordering may be observed. The fact that the appearance of a magnetic order occurs only above a minimum thickness of the magnetic layer has already been observed experimentally.[17]

Since the RKKY interaction oscillates with the argument $(k_F R)$, which depends on the carrier concentration, raising p produces a change in k_F, increasing the number of oscillations of J_{ij}^{RKKY}. Therefore, antiferromagnetic interactions can be turned on, resulting in all kinds of couplings. In this situation, ferromagnetic and antiferromagnetic interactions compete in establishing the magnetic order, which depends on the other sample characteristics, resulting in a total or in a partial alignment of the Mn magnetic moments. The occurrence of partial magnetization (about 40%) has also been observed in samples of (In,Mn)As/(Ga,Al)Sb.[41]

To conclude, we believe that the RKKY mechanism explains the high transition temperatures experimentally observed in $Ga_{1-x}Mn_xAs$ heterostructures, at least in the metallic phase. Additionally, it explains, as becomes clear after these Monte Carlo simulations, the occurrence of samples showing a partial magnetization at low temperatures. The possibility of having a ferromagnetic phase in samples with a low Mn concentration, i.e., in the ferromagnetic insulator $Ga_{1-x}Mn_xAs$, remains to be explained.

ACKNOWLEDGMENTS

This work was supported by CENAPAD-SP (Centro Nacional de Processamento de Alto Desempenho em São Paulo), UNICAMP/FINEP-MCT, CAPES, CNPq, and FAPERJ in Brazil, and by a PAST grant from the Ministère de l'Éducation Nationale, de l'Enseignement Supérieur et de la Recherche (France).

[1] J.K. Furdyna and J. Kossut, in *Diluted Magnetic Semiconductors*, edited by J.K. Furdyna and J. Kossut, *Semiconductors and Semimetals*, Vol. 24 (Academic Press, New York, 1988).

[2] T. Dietl, in *(Diluted) Magnetic Semiconductors*, edited by T.S. Moss, *Handbook of Semiconductors*, Vol. 3 (Elsevier, New York, 1994).

[3] A. Van Esch, L. van Bockstal, J. De Boeck, G. Verbank, A.S. van Steenbergen, P.J. Wellmann, B. Grietens, R. Bogaerts, F. Herlach, and G. Borghs, Phys. Rev. B **56**, 13 103 (1997).

[4] A. Van Esch, J. De Boeck, L. Van Bockstal, R. Bogaerts, F. Herlach, and G. Borghs, J. Phys.: Condens. Matter **9**, L361 (1997).

[5] A. Oiwa, S. Katsumoto, A. Endo, M. Hirasawa, Y. Iye, H. Ohno, F. Matsukura, A. Shen, and Y. Sugawara, Solid State Commun. **103**, 209 (1997).

[6] A. Shen, H. Ohno, F. Matsukura, Y. Sugawara, N. Akiba, T. Kuroiwa, A. Oiwa, A. Endo, S. Katsumoto, and Y. Iye, J. Cryst. Growth **175/176**, 1069 (1997).

[7] F. Matsukura, H. Ohno, A. Shen, and Y. Sugawara, Phys. Rev. B **57**, R2037 (1998).

[8] H. Ohno, N. Akiba, F. Matsukura, A. Shen, K. Ohtani, and Y. Ohno, Appl. Phys. Lett. **73**, 363 (1998).

[9] H. Ohno, F. Matsukura, T. Omiya, and N. Akida, J. Appl. Phys. **85**, 4277 (1999).

[10] H. Akai, Phys. Rev. Lett. **81**, 3002 (1998).

[11] J. Szczytko, A. Twardowski, K. Swiatek, M. Palczewska, M. Tanaka, T. Hayashi, and K. Ando, Phys. Rev. B **60**, 8304 (1999).

[12] M.A. Ruderman and C. Kittel, Phys. Rev. **96**, 99 (1954).

[13] T. Kasuya, Prog. Theor. Phys. **16**, 45 (1956).

[14] K. Yosida, Phys. Rev. **106**, 893 (1954).

[15] C. Kittel, in *Solid State Physics*, edited by F. Seitz, D. Turnbull, and H. Ehrenreich (Academic Press, New York, 1968), Vol. 22.

[16] L.G. Ferreira Filho, I.C. da Cunha Lima, and A. Troper, Semicond. Sci. Technol. **12**, 1592 (1997).

[17] T. Hayashi, M. Tanaka, K. Seto, T. Nishinaga, H. Shimada, and K. Ando, J. Appl. Phys. **83**, 6551 (1998).

[18] Y. Yafet, Phys. Rev. B **36**, 3948 (1987).

[19] Gerd Bergmann, William Shieh, and Mark Huberman, Phys. Rev. B **46**, 8607 (1992).

[20] P. Bruno and C. Chappert, Phys. Rev. Lett. **67**, 1602 (1991).

[21] D.M. Edwards, J. Mathon, R.B. Muniz, and M.S. Phan, Phys. Rev. Lett. **67**, 493 (1991).

[22] Frank Herman and Robert Schrieffer, Phys. Rev. B **46**, 5806 (1992).

[23] P. Bruno, Phys. Rev. B **52**, 411 (1995).

[24] J.S. Helman and W. Baltensperger, Phys. Rev. B **50**, 12 682 (1994).

[25] J.S. Helman and W. Baltensperger, Phys. Rev. B **53**, 275 (1996).

[26] I.S. Ibrahim and F.M. Peeters, Phys. Rev. B **52**, 17 321 (1995).

[27] I.Ya Korenblit and E.F. Shender, Zh. Éksp. Teor. Fiz. **69**, 1112 (1975) [Sov. Phys. JETP **42**, 566 (1975)].

[28] Ulf Larsen, Phys. Lett. **85A**, 471 (1981).

[29] M.T. Béal-Monod, Phys. Rev. B **36**, 8788 (1987).

[30] U. Gummich and I.C. da Cunha Lima, Solid State Commun. **76**, 831 (1990).

[31] D.N. Aristov, Phys. Rev. B **55**, 8064 (1997).

[32] T. Dietl, A. Haury, and Y. Merle d'Aubigné, Phys. Rev. B **55**, R3347 (1997).

[33] J. Szczytko, W. Mac, A. Twardowski, F. Matsukura, and H. Ohno, Phys. Rev. B **59**, 12 935 (1999), and references therein.

[34] A.A. Abrikosov, L.P. Gorkov, and I.E. Dzyaloshinsky, in *Methods of Quantum Field Theory in Statistical Physics*, edited by Richard A. Silverman (Dover, New York, 1963).

[35] *The Dielectric Function of Condensed Systems*, edited by L.V. Keldysh, D.A. Kirzhnitz, and A.A. Maradudin (Elsevier, New York, 1989).

[36] I.S. Gradshteyn and I.M. Ryzik, *Tables of Integrals, Series and Products*, revised edition (Academic Press, New York, 1980).

[37] M.A. Boselli, I.C. da Cunha Lima, and A. Ghazali, J. Appl. Phys. **85**, 5944 (1999).
[38] H.T. Diep, A. Ghazali, and P. Lallemand, J. Phys. C **18**, 5881 (1985).
[39] J. Okabayashi, A. Kimura, O. Rader, T. Mizokawa, A. Fujimori, T. Hayashi, and M. Tanaka, Phys. Rev. B **58**, R4211 (1998).
[40] A.K. Bhattacharjee and C. Benoit à la Guillaume, Solid State Commun. **113**, 17 (2000).
[41] A. Oiwa, A. Endo, S. Katsumoto, Y. Iye, H. Ohno, and H. Munekata, Phys. Rev. B **59**, 5826 (1999).